Hamedan University of Technology
Iranian Association of Electrical and Electronics Engineers

Sustainable Energy and Artificial Intelligence

Online ISSN: 3060-8015

Journal Homepage: www.enai.hut.ac.ir

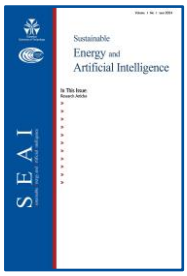

Water Balance and Management of a Proton Exchange Membrane Fuel Cell with Different Material Properties and Geometries

Iman Khazaee*, Hamid Sabadbafan

Faculty of Mechanical and Energy Engineering, ShahidBeheshti University, Tehran, Iran
** Corresponding Author: Imankhazaee@yahoo.com*

Article Info

Article type:
Original Article

Article history:
Received 2024-09-16;
Revised 2024-11-27;
Accepted 2024-12-24.

How to cite this article:
khazaee, I. and Sabadbafan, H. (2025). Water Balance and Management of a Proton Exchange Membrane Fuel Cell with Different Material Properties and Geometries. *Sustainable Energy and Artificial Intelligence*, *1*(1), 25-35.
DOI: 10.61186/seai.2409-1007

Abstract

While studying fuel cells, managing the amount of water and removing its excess, is crucial. Nano materials used in the membrane, catalyst and gas diffusion layers, as well as the thickness of those layers, could have different effects on water management and cell performance. In the current study, these issues were investigated theoretically with a Proton Exchange Membrane Fuel Cell (PEMFC) with 4-Serpentine flow channels. The geometries of the channels were rectangular and triangular, and the active area of the cell was 24.8cm^2. Pure Hydrogen and Oxygen were used on both sides. A complete three-dimensional and two-phase model was used for the numerical solution. To validate the solution, an experimental setup was designed to compare the simulation results with the experimental data, and the outcome was satisfactory. The aftermath shows an increased cell performance either by enhancing the thickness of the gas diffusion layers or reducing the thickness of the membrane in both rectangular and triangular channel geometry. Furthermore, under identical conditions, cell performance with rectangular channel is better than the one with the triangular channel.

***Keywords*:** Proton Exchange Membrane; Channel Geometry; Layer Thickness; 4-Serpentine; Energy.

Nomenclature

T_{ESS} (s)	The time constant related to the ESS	T_{ESS} (s)	The time constant related to the ESS
A_{active}	Active area of catalyst layer, m^2	S_m	Mass source term, kgm^{-3} s^{-1}
c_i	Concentration of species i, mol/m^3	T	Temperature, K
c_p	Specific heat of the mixture, J/kgK	S_l	Liquid water volume fraction
$D_{i,m}$	Diffusivity of i_{th} species in the mixture, m^2/s	Spc	Energy source term due to phase change, Wm^{-3}
F	Faraday's constant, 96,487C/mol	α	Charge transfer coefficient
n	Number of electrons transferred per mol of reactant	γ	Net water transport coefficient per proton
h_k	Enthalpy of k$_{th}$ phase, J/kg	ε	Porosity
h_{pc}	Latent heat of phase change, J/kg	$_m\mu$	Viscosity of the mixture, kg/ms

h_i	Enthalpy of i_{th} species, J/kg	*pc*	Phase change
i	Current density, A/m^2	ρ	Mixture density, kg/m^3
i_0	Exchange current density, A/m^2	δ	Thickness of the GDL, m
j	Transfer current density, A m^{-3}	*act*	Activation
J_i	Diffusion flux of i_{th} species, kgm^{-2}s	*cond*	Condensation
K	Permeability, m^2	*eff*	Effective
k_{cond}	Condensation rate constant, s^{-1}	*g*	Gas
k_{evap}	Evaporation rate constant, Pa^{-1}	*k*	liquid or gas phase
m	Mass, kg	*l*	Liquid
M_i	Molecular mass of species *i*, kgmol^{-1}	*m*	Mixture
p	Pressure, Pa	*sat*	Saturation
R	Universal gas constant, J/mol K	R_{ohmic}	Total electric resistance of cell, Ωcm^2

1. Introduction

Due to the increase of environmental concerns regarding air pollution, global warming and limited fossil fuels' resources, in the recent years many studies focused on using less polluting and renewable fuels. Because of high efficiency as well as no pollution, Hydrogen is taken under serious consideration among the different types of fuels and is being used in various types of fuel cells. In the current study, a Proton Exchange Membrane Fuel Cell (PEMFC), also called the Solid Polymer Fuel Cell (SPFC) [1], was applied.

A PEMFC typically includes the following components: a membrane, which separates anode and cathode parts; catalyst layer, which increases the rate of chemical reactions; gas diffusion layers and gas flow channels. The protons pass through the membrane into the cathode catalyst layer, and electrons pass through an external circuit so an external electrical current is created. Fuel and oxygen pass through gas flow channels and then pass the porous parts of the gas diffusion layer and move to the catalyst layer.In reading the literature one could see lots of researches using either experimental or theoretical method to study fuel cells in detail [9]. Since in the current paper the modeling method is employed, more emphasis is on this approach.In recent years, some research has been done to investigate the influence of different parts of PEMFCs on the cell performance. A certain amount of them are summarized here:

S. Rowshanzamir et al. [10], developed a mathematical model for the catalyst layer in the cathode electrode side. Their model was one dimensional, isothermal and pseudo-homogeneous. They reported that as the active area of catalyst surface increases, the current density increases. Furthermore, they founded that an increase in the proton conductivity, leads to a decrease in the variation of over potential across the catalyst layer as well as a decrease in the catalyst layer effective thickness.In another work, Agus et al. [11], numerically evaluated the performance of various gas and coolant channel designs simultaneously. They also introduced a hybrid parallel-serpentine-oblique-fins design for a PEMFC, which they claimed to have a better performance compared to conventional channels.

In a similar work, Lei et al. [12], investigated a model for PEMFC. It was a two-dimensional model in which the temperature distribution was modeled non-isothermal, water transport was simulated using two-phase flow model and the agglomerate model was used for Oxygen consumption. It should be noted that all the models were full coupled, in order to study the thermal and water transport. They reported that higher operating temperature increased the cell performance. A more thorough work was done by Rostami et al. [13], to investigate the effect of bend sizes on a PEMFC. It was shown that as bend size increased from 1mm to 1.2mm, both the over potential loss and the temperature gradient were reduced. They also reported that the 1.2mm bend size compared to the 0.8mm one, impeded the secondary flow more successfully which resulted in a 90.6% reduction in the pressure drop.

To investigate the effects of compression on the water management, Zhongying Shi, et al. [14], coupled a finite-element compression model with a steady-state fuel cell model. They observed that both the porosity and permeability of the GDL decreased after the compression, especially under the shoulder of the bipolar plate. Some other models were also developed to investigate the behavior of fuel cells under different conditions[15-22], for example,a two-dimensional CFD model was developed by Tiss et al. [15].

In the current paper, the effect of several factors on the water balance and the cell performance of a PEMFC were studied. The material properties of membrane, catalyst layers as well as gas diffusion layers were the variable parameters. PEMFCs with 4-Serpentine flow

channels and both rectangular and triangular geometries have been evaluated. In the following parts first, a brief description of the experiments will be expressed, and then the numerical model will be explained.

2. Description of the Experiments

In order to investigate the performance of the fuel cell experimentally, a set up was fabricated. The setup could measure and display the temperature, the inlet or outlet rate and pressure of both hydrogen as well as oxygen. A schematic flow of the test bench is shown in Fig. 1. The characteristics of the measurement devices are shown in Table 1. Furthermore, the operating conditions of the cell are listed in Table 2.

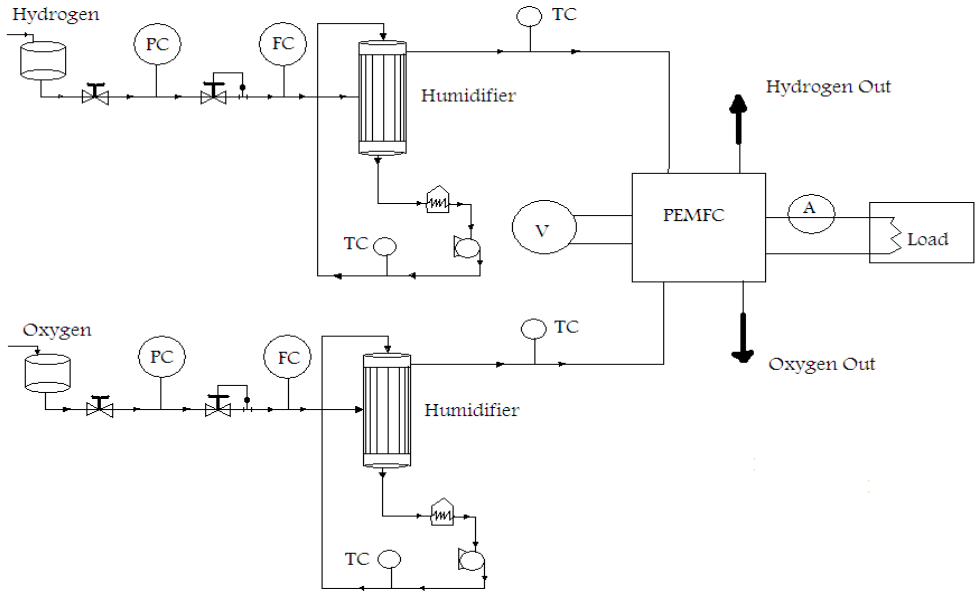

Fig. 1.The schematic of the PEMFC setup used for the experiments.

Table 1. Characteristics of the measurement devices

	Model	Range	Accuracy
Pressure regulator	Q1-202-510A	0–16 bar	±2 %
Flow meter	LZB-4WB	0–3 L/min	±0.1 L/min
Thermometer of cell	TC4S	0.1–1000 °C	±0.1 °C
Thermometer of gases	TX3	−40 to 100 °C	±0.1 °C
Voltmeter	ELB350	0–15 V	±0.1 V
Ampere meter	ELB350	0–20 A	±0.1 A

Table 2. Operating conditionsduring the experiments

Parameters	Value	Units
Operation pressure	290.5	KPa
Operation temperature	60	℃
Relative humidity	100%	-
Mass flow rate of Hydrogen	4.065×10^{-7}	Kg/s
Mass flow rate of Oxygen	1.076×10^{-5}	Kg/s

3. Numerical Model

The numerical model in the current study included the following conditions:

- The geometry of anode and cathode layer was either triangular or rectangular.
- The gas diffusion layer on both sides had three different thickness: 0.23mm, 0.33mm and 0.43mm.
- The catalyst layer in both anode and cathode sides had three different thickness: 0.005mm, 0.01mm and 0.15mm.
- The proton exchange membrane had three different thickness: 0.041mm, 0.051mm and 0.061mm.
- Hydrogen and Oxygen passed through 4-Serpentine flow channels.
- The active area was 2480mm^2.
- For rectangular geometry, the channel depth and width were both 1mm.
- For triangular geometry, the channel depth and width were respectively 2mm and 1mm.

The schematic diagram of flow channelsas well as the inflow and outflow regions for Hydrogen and Oxygen, in both geometries are shown in Fig. 2.

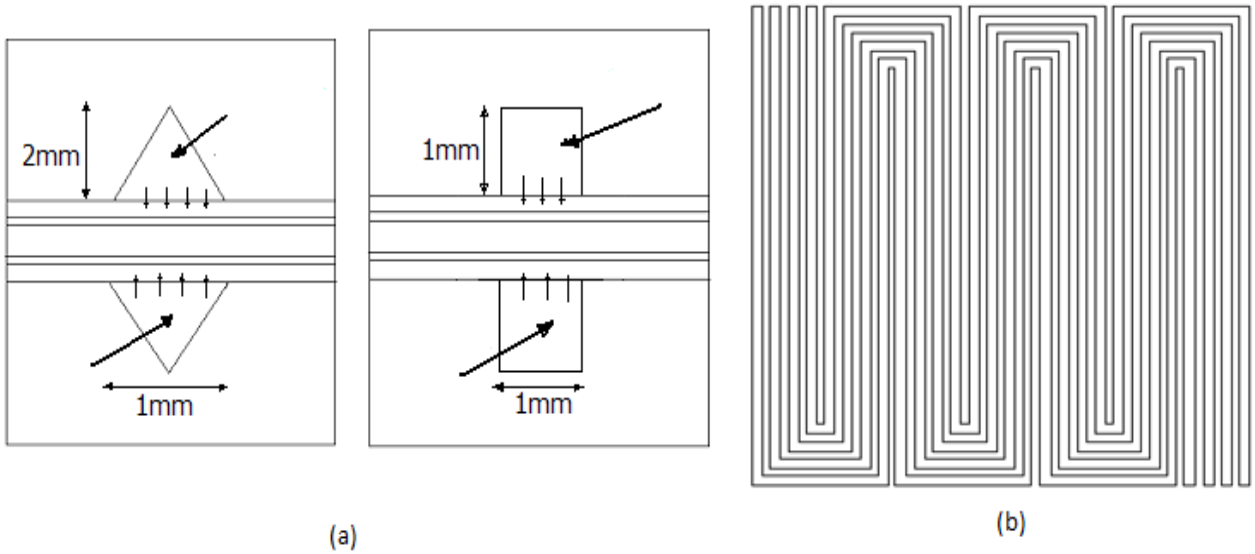

Fig. 2. (a) The inflow and outflow regions for triangle and rectangular geometries, (b)The schematic diagram of flow channels

It was assumed that the inlet reactants were ideal gases, and the flow was laminar. The porous layers such as GDL, CL and PEM were assumed to be isotropic. Homogeneous two-phase flow assumption was considered, and both the liquid and gas phases were supposed to move at the same velocity. This assumption holds for normal operating conditions of a PEMFC because high liquid loadings will not allow steady-state operation [23]. Theoretical fundamentals and formulas which were used in modeling can be summarized as follows:

3-1. Mass Conservation

Equation 1 could be applied for mass conservation in a fuel cell.

$$\nabla.(\varepsilon\,\rho_m\overline{u_{\mathrm{m}}}) = \mathrm{s}_m \tag{1}$$

Where ε is the porosity, $\rho_m$is the mixture density and$\bar{u}_m$is the average velocity of the mixture. S_m is calculated according to Equation (2).

$$\begin{aligned}\mathrm{s}_m &= \mathrm{s}_{\mathrm{O}_2} + \mathrm{s}_{\mathrm{H}_2O} + \mathrm{s}_{pc}\\ &= \left(\frac{-\mathrm{i}}{4\mathrm{F}}M_{\mathrm{O}_2} + \frac{\mathrm{i}(1+2\gamma)}{2\mathrm{F}}.M_{\mathrm{H}_2O}\right).\frac{\mathrm{A\ active}}{\mathrm{V}} + \mathrm{s}_{pc}\end{aligned} \tag{2}$$

Where $\boldsymbol{s_{O_2}}$ presents the Oxygen consumption at the cathode catalyst layer, and $\boldsymbol{s_{H_2O}}$ is the production of steam. iis the local current density. $\boldsymbol{M_{O_2}}$ and $\boldsymbol{M_{H_2O}}$ are the molecular mass of Oxygen and Hydrogen. F is the Faraday's constant; A is the active aria and V is the volume of the catalyst layer. The net water transported to cathode side due to electro-osmotic drag and concentration gradient is accounted by the water transport coefficient $\boldsymbol{\gamma}$. It should be noted that only the water phase change term is presented in GDL and gas channels. If the partial pressure of water vapor exceeds the local saturation pressure corresponding to the local temperature, condensation will take place. This phase-change phenomenon is modeled using the following equations.

$$\begin{aligned}s_{pc} = \dot{m_{pc}} &= k_{cond}.(1-s_l).\frac{M_{H_2O}}{RT}.P.\left(X_g^{H_2O} - X_{sat}^{H_2O}\right)\\ &\qquad if \quad X_g^{H_2O} \geq X_{sat}^{H_2O}\end{aligned} \tag{3}$$

$$\begin{aligned}\mathrm{s}_{pc} = \dot{m_{pc}} &= \mathrm{k}_{\mathrm{evap}}.s_l.\rho_l.P.\left(X_g^{H_2O} - X_{sat}^{H_2O}\right)\\ &\qquad if \quad X_g^{H_2O} \geq X_{sat}^{H_2O}\end{aligned} \tag{4}$$

The saturation pressure for the fuel cell temperature range could be calculated using Equation (5):

$$\begin{aligned}\mathrm{P}_{sat} = &-2846.4 + 411.24 \times (T - 273.15)\\ &- 10.554 \times (T - 273.15)^2\\ &+ 0.16636 \times (T - 273.15)^3\end{aligned} \tag{5}$$

The conservation equation for the liquid phase was set as follows:

$$\nabla.(\varepsilon s_l \rho_l \overline{u_{\mathrm{m}}}) = \mathrm{s}_{PC} \tag{6}$$

Where $\boldsymbol{s_l}$ is the liquid phase volume fraction, $\boldsymbol{\rho_l}$ is the density of the liquid water and the term $\boldsymbol{\overline{u_m}}$, is calculated using Equation (7):

$$\overline{u}\mathrm{m} = \sum_{k=l,g}\frac{s_k\rho_k\overline{u}_k}{\rho_m} \tag{7}$$

Where $\boldsymbol{s_k}$, represents the volume fraction of phase k in the control volume [24].

The relations used for calculating the properties of the gaseous phase and two-phase mixture are given in Table 3 and the different source terms appearing in governing equations at different domains are given in Table 4.

Table 3. Relations used for calculating the gaseous and two-phase mixture properties [16]

	Density	Viscosity	Thermal conductivity
Gas mixture(H_{2o},o_2)	$\rho_g=\frac{p}{RT\sum_i \frac{y_i}{M_i}}$	$\mu_g=\sum_i \frac{x_i\mu_i}{\sum_j x_i \emptyset_{ij}}$ $\emptyset_{ij}=\frac{[1+(\frac{\mu_i}{\mu_j})^{0.5}(\frac{M_j}{M_i})^{0.25}]^2}{[8(1+\frac{M_j}{M_i})]^{0.5}}$	$k_g=\sum_i \frac{x_i k_i}{\sum_j x_i \emptyset_{ij}}$ $\emptyset_{ij}=\frac{[1+(\frac{\mu_i}{\mu_j})^{0.5}(\frac{M_j}{M_i})^{0.25}]^2}{[8(1+\frac{M_j}{M_i})]^{0.5}}$
Two phase mixture	$\rho_m=\sum_{k=l,g} s_k \rho_k$	$\mu_m=\sum_{k=l,g} s_k \mu_k$	$k_m=\sum_{k=l,g} s_k k_k$

Table 4. Source terms in different regions of computational domain

Domain	Mass source term	Momentum source term	Energy source term	Species source term	S_k	$s_\emptyset$
`	$S_{o2}+S_{H2o}+S_{pc}$	S_M	$(\frac{T\Delta s}{2F}+V_{act})i\frac{A_{act}}{V}+\dot{m_{pc}}h_{pc}$	$S_{o2}+S_{H2o}+S_{pc}$	$-\frac{j_a}{2F}\frac{\rho}{\varepsilon_{m}\varepsilon_{mc}}$: anode H_2 $-\frac{j_c}{2F}\frac{\rho}{\varepsilon_{m}\varepsilon_{mc}}$: cathode$O_2$ $-\frac{j_c}{F}(\frac{1}{2}+n_d)\frac{\rho}{\varepsilon_{m}\varepsilon_{mc}}$:cathode$H_2O$ $-j_a\frac{n_d}{F}\frac{\rho}{\varepsilon_{m}\varepsilon_{mc}}$: anode$H_2O$	j
GDL	S_{pc}	S_M	$\dot{m_{pc}}h_{pc}$	S_{pc}	0	0
Channels	S_{pc}	-	$\dot{m_{pc}}h_{pc}$	S_{pc}	0	0

3-2. Momentum Conservation

Equation (8) could be applied for momentum conservation in a fuel cell.

$$\nabla.(\varepsilon\,\rho_m\overline{u_m}.\overline{u_m}) = -\varepsilon\,\nabla P + \nabla.(\varepsilon\,\mu_m\nabla\overline{u_m}) + S_M \quad (8)$$

Where $\boldsymbol{P}$ is the pressure and $\boldsymbol{\mu_m}$ is the dynamic viscosity of the mixture.According to Darcy's model for viscous drag, due to the interaction between the fluid and porous gas diffusion layer and catalystlayer,it could be writen:

$$S_M = -\left(\frac{\mu_m\overline{u_m}}{k}\right) \quad (9)$$

Where $\boldsymbol{k}$ is the permeability of the porous layer.

3-3. Species Conservation

Assuming the diffusive transport follows Fick's law, it is given by:

$$\nabla.(\varepsilon\,\rho_m\overline{u}_m y_i) = \nabla.(\varepsilon\,\rho_m D_{i,m}^{eff}\nabla y_i) + S_i \quad (10)$$

Where $\boldsymbol{y_i}$, is the mass fraction of species $\boldsymbol{i}$. The source term $\boldsymbol{S_i}$ represents the Oxygen consumption and water generation in the catalyst layer as well as the phase change phenomena in the CL, GDL and gas channels [24].

3-4. Energy Conservation

Equation (11) could be applied for energy conservation in a fuel cell.

$$\nabla.\sum_{k=l,g}(\varepsilon\,S_k\rho_k h_k\overline{u}_k) = \nabla.(k_{eff}\nabla T - \sum_i h_i J_i) + S_E \quad (11)$$

Where h_k and h_i are respectively the sensible enthalpy of phase k and the enthalpy of the species, which are calculated according to Equations (12) and (13):

$$h_k = \sum_i y_i\, h_i \quad (12)$$

$$h_i = \int_{298.15}^{T} C_{p,i}\mathrm{d}T \quad (13)$$

At the energy equation (Equation (11)), the first term on the right-hand side represents the energy transport due to conduction where $\boldsymbol{k_{eff}}$ is the effective thermal conductivity of the porous media and can be calculated as follows:

$$k_{eff} = \varepsilon\,k_m + (1-\varepsilon)k_s \quad (14)$$

The second term presents the energy transport due to species diffusion, where $\boldsymbol{J_i}$ is the species diffusion flux and finally, $\boldsymbol{S_E}$ is the energy source term which involves the released heat from the reaction as well as the latent heat of phase change, and it can be given by:

$$S_E = (\frac{T\Delta S}{2F}+\Delta V_{act})\,i\frac{A_{act}}{\overline{V}} + \dot{m_{pc}}h_{pc} \quad (15)$$

In the above equation, the irreversible loss in energy conversion, which is due to change in entropy during the reaction, is accounted by the first term.The second term is equal to the energy spent to overcome the activation barrier at the electrode-electrolyte interface. The last term, $\boldsymbol{\dot{m}_{pc}h_{pc}}$, is the heat transfer associated with water phase change, where $\boldsymbol{\dot{m}_{pc}}$ is the mass transferred

between the phases, and h_{pc} is a function of temperature and can be calculated as follows:

$$h_{pc} = 3.0709 \times 10^5 (647.15 - \mathrm{T})^{0.35549} \quad (16)$$

3-5. Electrochemical Model

Current density can be calculated as a function of Oxygen concentration along the catalyst layer, using Butler-Volmer's equation:

$$i = (1 - \mathrm{s_l}) \frac{i_o}{c_{o_{2,ref}}} \frac{\rho_m y_{o_2}}{M_{o_2}} \exp\left(\frac{4\alpha F}{RT}\eta\right) \quad (17)$$

Where the term $(1 - s_l)$, is the reduced activity level due to the formation of water, i_o is the cathode exchange current density, $c_{o_{2,ref}}$ is the reference oxygen concentration at the electrode, α is the charge transport coefficient, which represents the symmetry of the activation barrier at the electrode-electrolyte interface, R is the universal gas constant, T is the local temperature and η is the activation over potential, which drives the reaction. Celloperating voltage can also be calculated using the following equation:

$$V_{cell} = V_o - \Delta V_{act} - \Delta V_{ohmic} - \Delta V_{conc} \quad (18)$$

In the above equation, V_o is open circuit potential, ΔV_{act} is the activation voltage loss, ΔV_{ohmic} is the ohmic voltage loss and ΔV_{conc} is the concentration voltage loss. Each of these terms can be calculated using the following equations:

$$V_o = \mathrm{V_{TD}} + \frac{\Delta S}{nF}(\mathrm{T} - \mathrm{T_0}) - \frac{RT}{nF}\ln\left(\frac{p_{H_2O}}{p_{o_2}^{1/2}}\right) \quad (19)$$

$$\Delta V_{act} = \frac{RT}{\alpha F} \ln\left(\frac{i}{i_o}\right) = \eta \quad (20)$$

$$\Delta V_{ohmic} = \mathrm{i} R_{ohmic} \quad (21)$$

$$\Delta V_{conc} = \frac{RT}{nF}\left(1 + \frac{1}{\alpha}\right) \ln\left(\frac{i_L}{i_L - i}\right) \quad (22)$$

In Equation (19), V_{TD} is the standard state reversible voltage and the second and third terms respectively,represent the variation in reversible voltage due to changes in temperature and partial pressure of reactants. Equation 20, will be used if the activation voltage loss is considered in the cathode. In the above equations, i is the current density and R_{ohmic} is the total cell ohmic resistance. The limiting current density i_L is the maximum current density that can be obtained from a fuel cell under a particular set of operating conditions and can be calculated as follows:

$$i_L = \frac{nF D_{i,m}^{eff} C_{Bulk,O_2}}{\delta} \quad (23)$$

Where C_{Bulk,O_2} is the bulk concentration of oxygen in the channels and δ is the thickness of the diffusion layer. The effect of porosity on the diffusion of reactant species through porous GDL and CL is consideered using the Bruggeman relation. The equation gives the effective diffusivity of a species in the mixture ($D_{i,m}^{eff}$) as a function of porosity ε and tortuosity τ of the porous material and the liquid volume fraction s_l:

$$D_{i,m}^{eff} = [(1 - s_l)\varepsilon]^{\tau} D_{i,m} \quad (24)$$

Where $D_{i,m}$ is the diffusivity of species i in the mixture [24].

It should be noted that, both generation or consumption of chemical species k and the creation of electrical current occur only at the active catalyst layers, where electrochemical reactions take place [25].

The whole computational domain in the present study contains 1149300 grid cells for rectangular geometry and 1198191 grid cells for triangular geometry. The solution is considered to be converged when the difference between successive iterations is less than 10^{-6} for all variables. Pure Hydrogen and Oxygen are used as reactant gases in the model. The electrochemical and transport parameters used in these simulations are summarized in Table 5.

Table 5. Electrochemical and transport properties used in the simulations.

parameters	unit	amount
Anode reference exchange current density	A/m^2	1500000000
Cathode reference exchange current density	A/m^2	4000000
Anode transfer coefficient		2
Cathode transfer coefficient		2
Faraday constant	C mol^{-1}	96487
H_2 Diffusivity	$m^2 s^{-1}$	0.00003
O_2 Diffusivity	$m^2 s^{-1}$	0.00003
H_2O Diffusivity at anode	$m^2 s^{-1}$	0.00003
H_2O Diffusivity at cathode	$m^2 s^{-1}$	0.00003
Anode backing layer porosity		0.5
Cathode backing layer porosity		0.5
Permeability of anode backing layer	m^2	0.000000000001
Permeability of cathode backing layer	m^2	0.000000000001
Equivalent weight of membrane	kg mol^{-1}	1.1

Using the numerical model, which was explained in detail previously, the performance of the fuel cell and the content of water for both rectangular and triangular geometries were simulated. The simulation results were calculated for different thickness of layers, and the effects on the cell output were evaluated. In the following part, at the beginning, the experimental model used for validation of the numerical model, will be introduced and then the results for both

experimental and numerical models under various operating conditions will be compared.

4. Results and Discussion

To validate the model, the cell performance data obtained from the numerical simulation were compared with the experimental data. The experimental data were obtained by testing a fuel cell with 4-serpentine channel. The operating conditions for numerical model and experimental model are presented in Table 2. The comparison of results are illustrated in Fig. 3. As it can be seen, the computed polarization curve concurs with the experimental one.

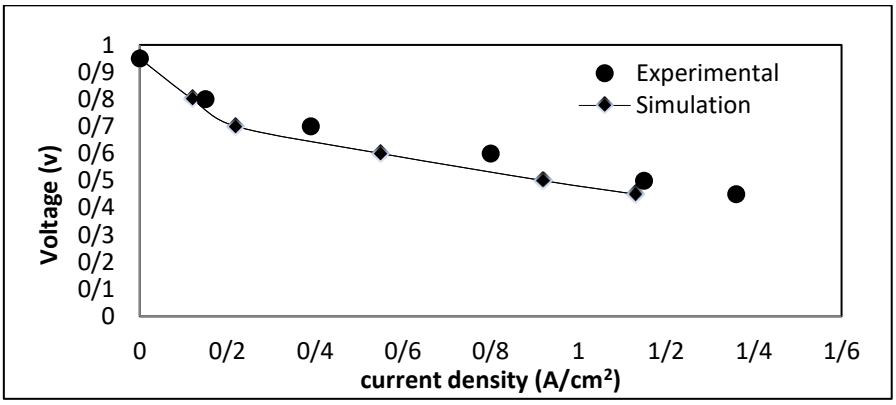

Fig. 3. Comparison of simulation results with the experimental data for cell with rectangular channel

To analyze the influence of membrane layer thickness on cell performance, polarization curves for voltage with current density were generated for membrane thicknesses of 0.041mm, 0.051mm, and 0.061mm, as depicted in Fig. 4. Figs. 4a and 4b illustrate the results for rectangular and triangular geometries, respectively. These figures reveal a notable trend: as membrane thickness decreases, performance improves across both geometries, particularly in the regions of the polarization curves affected by Ohmic losses.

This enhancement in performance is largely attributable to a reduction in charge transfer resistance associated with thinner membranes, which facilitates more efficient ion conduction across the membrane. A thinner membrane layer enables shorter proton pathways, reducing resistance and thus enhancing the overall conductivity of the cell. Consequently, optimizing membrane thickness emerges as a critical factor for achieving lower Ohmic losses and higher overall efficiency in both geometric configurations of the proton exchange membrane fuel cell (PEMFC).

Fig. 5 and Fig. 6, show contours of liquid water content in the membrane for cell with rectangular and triangular geometry at different membrane layer thickness and RH=%100 and V=0.7V. The lower the membrane thickness, the higher the amount of water absorption at the membrane, which as a result, more ionic clusters or channels are filled with water. Therefore, protons as free ions can transport easily through these water-filled clusters or ionic channels inside the polymer membrane networks. This results in a lower membrane resistance through the cell with thinner membrane.

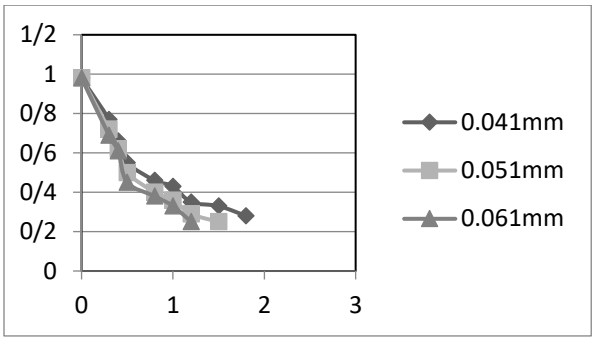

(a)

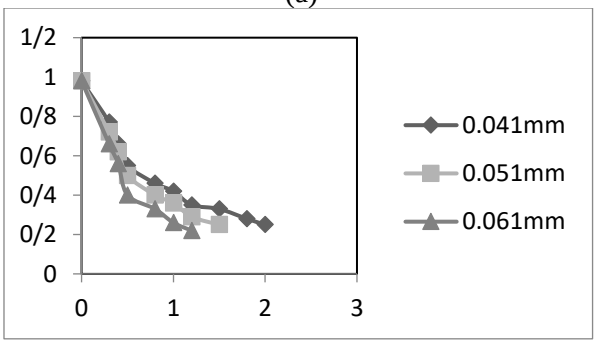

(b)

Fig. 4. (a) Effect of membrane layer thickness for a cell with rectangular geometry; T=60℃, $\dot{m}O_2$=0.5 Lmin^{-1}, $\dot{m}H_2$ =0.3Lmin^{-1}, p=2.905 bar and RH=%100. (b) Effect of membrane layer thickness for a cell with triangular geometry; T=60℃, $\dot{m}O_2$=0.5 Lmin^{-1}, $\dot{m}H_2$ =0.3 Lmin^{-1}, p=2.905 bar and RH=%100

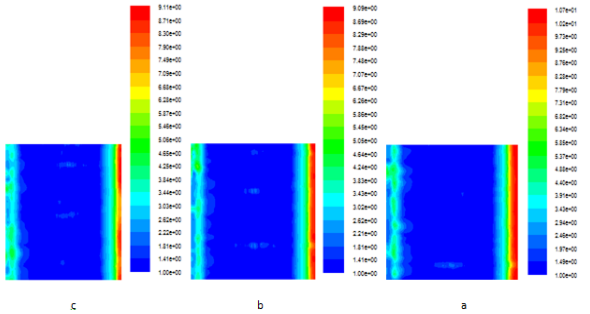

Fig. 5. Contours of liquid water content distribution in the membrane for cell with rectangular geometry (V=0.7V, RH=%100): (a) Membrane thickness= 0.041mm; (b) Membrane thickness= 0.051mm; (c) membrane thickness=0.061mm.

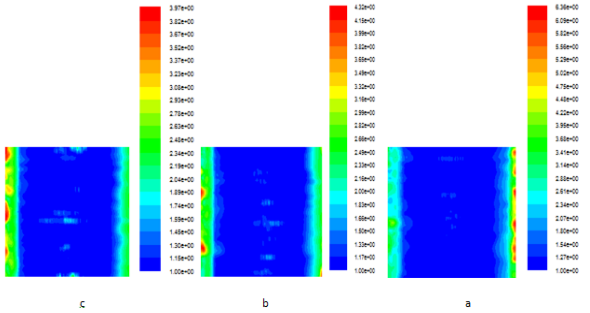

Fig. 6. Contours of liquid water content distribution in the membrane for cell with triangular geometry (V=0.7V, RH=%100): (a) Membrane thickness= 0.041mm; (b) Membrane thickness= 0.051mm; (c) Membrane thickness=0.061mm

The effect of catalyst layer thickness on cell performance was examined for both anode and cathode sides, as shown in Fig. 7. for voltage with current density For cells with triangular geometry, an increase in catalyst layer thickness led to enhanced performance across all voltage levels. In contrast, the rectangular geometry exhibited a more complex behavior: at voltages below 0.4V, performance declined with increasing catalyst layer thickness, but at voltages above 0.4V, performance aligned with that of the triangular geometry. This difference can be attributed to the role of water in the catalyst layer, where the hydrated ion clusters and channels within the polymer facilitate gas diffusion.

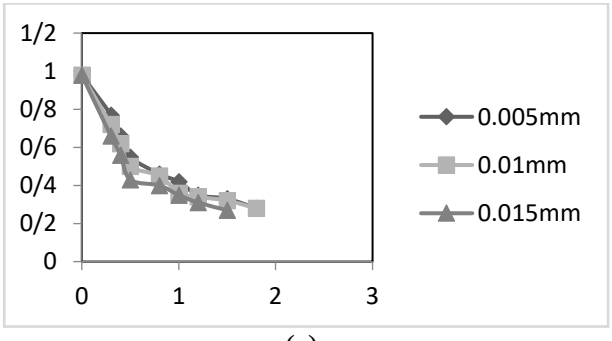

(a)

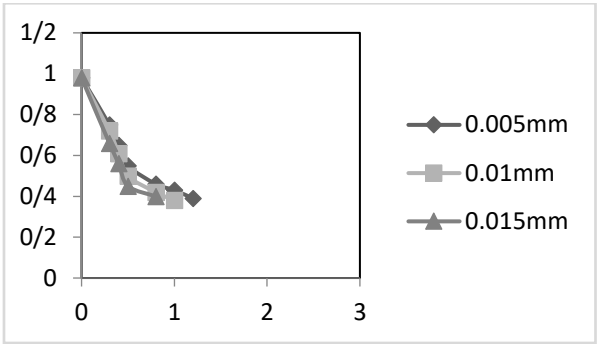

(b)

Fig. 7. (a) Effect of catalyst layers thickness for a cell with rectangular geometry; T=60℃, $\dot{m}O_2$=0.5 Lmin^{-1}, $\dot{m}H_2$ =0.3 Lmin^{-1}, p=2.905 bar and RH=%100 (b) Effect of catalyst layers thickness for a cell with triangular geometry; T=60℃, $\dot{m}O_2$=0.5 Lmin^{-1}, $\dot{m}H_2$ =0.3 Lmin^{-1}, p=2.905 bar and RH=%100.

As catalyst layer thickness decreases, the water content within the layer reduces, resulting in dehydration of the ionomer. This dehydration impacts the transport properties, reducing both the permeability of hydrogen and oxygen and the amount of dissolved oxygen, thus affecting the electrochemical reaction rate and cell performance. Figs. 8 and 9 display the distribution of current density across the cathode catalyst layer for rectangular and triangular geometries with varying catalyst layer thicknesses (0.005mm, 0.01mm, and 0.015mm) under conditions of 100% relative humidity and a voltage of 0.7V. These figures demonstrate a clear trend: higher water content within the catalyst layer correlates with increased current density, highlighting the significant influence of water management on enhancing reaction rates and, consequently, performance.

Additionally, the impact of gas diffusion layer (GDL) thickness on cell performance was investigated . As illustrated in Fig. 10, for voltage with current density, increasing GDL thickness (tested at 0.23mm, 0.33mm, and 0.43mm) led to improved performance for both rectangular and triangular geometries. However, this effect was more pronounced in rectangular geometries. This outcome suggests that thicker GDLs improve water management by facilitating optimal gas diffusion and water retention, thereby contributing to enhanced overall cell efficiency. These findings underline the critical role of water management in the design and optimization of proton exchange membrane fuel cells (PEMFCs), confirming that careful consideration of material properties and structural design is essential for maximizing cell performance.

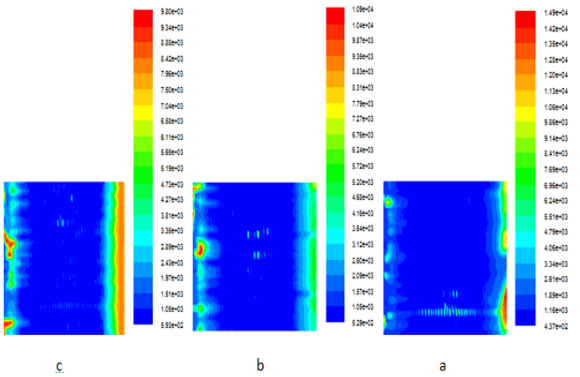

Fig. 8. Contours of current density (A/m^2) in the cathode catalyst layer for cell with rectangular geometry (V=0.7V, RH=%100): (a) Catalyst layers thickness= 0.005mm; (b) Catalyst layers thickness= 0.01mm; (c) Catalyst layers thickness=0.015mm

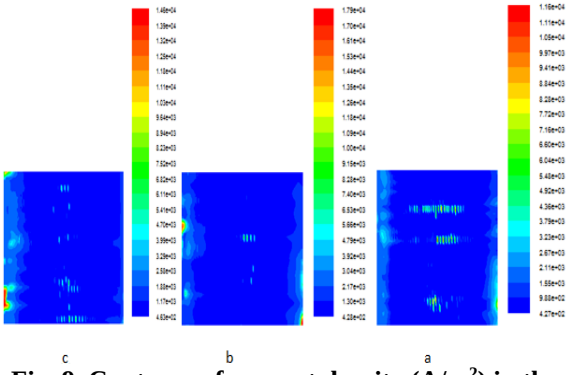

Fig. 9. Contours of current density (A/m^2) in the cathode catalyst layer for cell with triangular geometry (V=0.7V, RH=%100): (a) Catalyst layers thickness= 0.005mm; (b) Catalyst layers thickness= 0.01mm; (c) Catalyst layers thickness=0.015mm.

5. Conclusion and Recommendations

To meet energy demands and reduce pollution, expanding the use of fuel cell systems is essential. A major challenge in using fuel cell technology lies in water management, which is directly correlated with system performance. In this study, a comprehensive three-dimensional, two-phase model of a Proton Exchange Membrane Fuel Cell (PEMFC) with a 4-serpentine channel design was developed, incorporating both rectangular and triangular geometries. The effects of varying the thickness of different cell layers on water management and performance were investigated, using pure hydrogen and oxygen as reactant gases.

The findings confirmed that layer thickness significantly influences PEMFC output. Generally, performance increased with either a reduction in membrane layer thickness or an increase in gas diffusion layer thickness for both geometries. Additionally, performance changes with gas diffusion layer thickness were more pronounced in rectangular channels than in triangular ones. In cells with rectangular channels, increasing the catalyst layer thickness improved performance only at voltages above 0.4V, whereas in triangular channels, this improvement was observed across all simulated voltages.

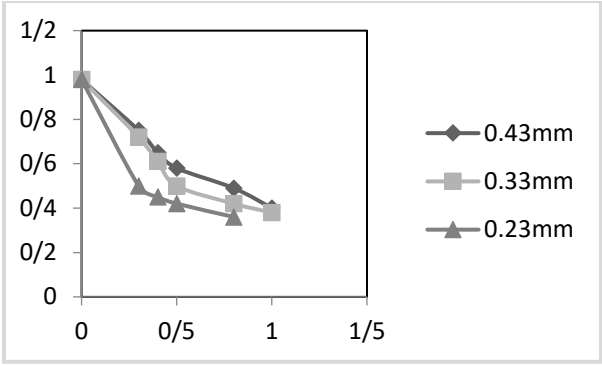

(a)

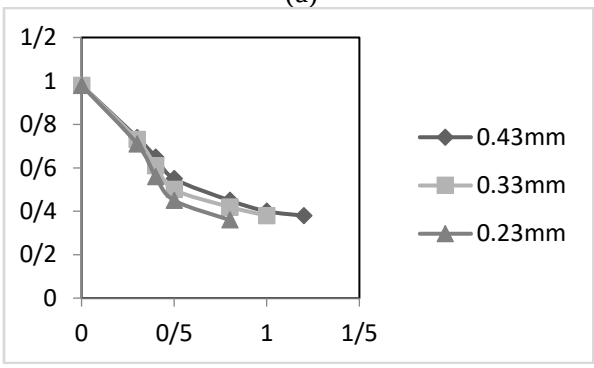

(b)

Fig. 10. (a) Effect of gas diffusion layer thickness for a cell with rectangular geometry; T=60℃, $\dot{m}O_2$=0.5 Lmin^{-1}, $\dot{m}H_2$ =0.3 Lmin^{-1}, p=2.905 bar and RH=%100 (b) Effect of gas diffusion layer thickness for a cell with rectangular geometry; T=60℃, $\dot{m}O_2$=0.5 Lmin^{-1}, $\dot{m}H_2$ =0.3 Lmin^{-1}, p=2.905 bar and RH=%100 (b) Effect of gas diffusion layer thickness for a cell with triangular geometry; T=60℃, $\dot{m}O_2$=0.5 Lmin^{-1}, $\dot{m}H_2$ =0.3 Lmin^{-1}, p=2.905 bar and RH=%100

The computational domain included 1,149,300 grid cells for the rectangular geometry and 1,198,191 for the triangular geometry. Convergence was achieved when the difference between successive iterations for all variables was less than10^6. An experimental setup was also prepared to validate the simulation results, showing good agreement between the modeled and measured data.

This study highlights that water management is a critical aspect in designing efficient PEMFCs, underscoring the need for further research to optimize layer thickness for improved performance.

References

[1] Larminie, J., Dicks, A., & McDonald, M. S. (2003). *Fuel cell systems explained* (Vol. 2, pp. 207-225). Chichester, UK: J. Wiley.

[2] Thomas, S., Vang, J. R., Araya, S. S., & Kær, S. K. (2017). Experimental study to distinguish the effects of methanol slip and water vapour on a high temperature PEM fuel cell at different operating conditions. *Applied Energy*, *192*, 422-436.

[3] Li, J., Li, X., Yu, S., Hao, J., Lu, W., Shao, Z., & Yi, B. (2014). Porous polybenzimidazole membranes doped with phosphoric acid: Preparation and application in high-temperature proton-exchange-membrane fuel cells. *Energy conversion and management*, *85*, 323-327.

[4] Liso, V., Araya, S. S., Olesen, A. C., Nielsen, M. P., & Kær, S. K. (2016). Modeling and experimental validation of water mass balance in a PEM fuel cell stack. *International Journal of Hydrogen Energy*, *41*(4), 3079-3092.

[5] Heidary, H., Kermani, M. J., Advani, S. G., & Prasad, A. K. (2016). Experimental investigation of in-line and staggered blockages in parallel flowfield channels of PEM fuel cells. *International journal of hydrogen energy*, *41*(16), 6885-6893.

[6] Zakaria, I., Azmi, W. H., Mamat, A. M. I., Mamat, R., Saidur, R., Talib, S. A., & Mohamed, W. A. N. W. (2016). Thermal analysis of Al2O3–water ethylene glycol mixture nanofluid for single PEM fuel cell cooling plate: an experimental study. *International Journal of Hydrogen Energy*, *41*(9), 5096-5112.

[7] Bvumbe, T. J., Bujlo, P., Tolj, I., Mouton, K., Swart, G., Pasupathi, S., & Pollet, B. G. (2016). Review on management, mechanisms and modelling of thermal processes in PEMFC. *Hydrogen and Fuel Cells*, *1*(1), 1-20.

[8] Wu, H. W. (2016). A review of recent development: Transport and performance modeling of PEM fuel cells. *Applied energy*, *165*, 81-106.

[9] Daud, W. R. W., Rosli, R. E., Majlan, E. H., Hamid, S. A. A., Mohamed, R., & Husaini, T. (2017). PEM fuel cell system control: A review. *Renewable Energy*, *113*, 620-638.

[10] Rowshan,Z. S., Eikani, M., Khoshnoodi, M., & Eshagh N. T. (2008). A parametric study of the PEM fuel cell cathode. *IUST Int. J. of Engineering Science*, *19*(2-5), 73-81.

[11] Sasmito, A. P., Kurnia, J. C., & Mujumdar, A. S. (2012). Numerical evaluation of various gas and coolant channel designs for high performance liquid-cooled proton exchange membrane fuel cell stacks. *Energy*, *44*(1), 278-291.

[12] Xing, L., Liu, X., Alaje, T., Kumar, R., Mamlouk, M., & Scott, K. (2014). A two-phase flow and non-isothermal agglomerate model for a proton exchange membrane (PEM) fuel cell. *Energy*, *73*, 618-634.

[13] Rostami, L., Nejad, P. M. G., & Vatani, A. (2016). A numerical investigation of serpentine flow channel with different bend sizes in polymer electrolyte membrane fuel cells. *Energy*, *97*, 400-410.

[14] Shi, Z., Wang, X., & Guessous, L. (2010). Effect of compression on the water management of a proton exchange membrane fuel cell with different gas diffusion layers. *Journal of fuel cell science and technology*, *7*(2), 021012.

[15] Tiss, F., Chouikh, R., & Guizani, A. (2013). A numerical investigation of the effects of membrane swelling in polymer electrolyte fuel cells. *Energy conversion and management*, *67*, 318-324.

[16] Perng, S. W., Wu, H. W., & Wang, R. H. (2014). Effect of modified flow field on non-isothermal transport characteristics and cell performance of a PEMFC. *Energy conversion and management*, *80*, 87-96.

[17] Abdollahzadeh, M., Pascoa, J. C., Ranjbar, A. A., & Esmaili, Q. (2014). Analysis of PEM (Polymer Electrolyte Membrane) fuel cell cathode two-dimensional modeling. *Energy*, *68*, 478-494.

[18] Ruksawong, K., Songprakorp, R., Monyakul, V., David, N. A., Sui, P. C., & Djilali, N. (2017). Investigation of PEMFC under Static Magnetic Field: Temperature, Relative Humidity and Performance. *Journal of The Electrochemical Society*, *164*(2), F1-F8.

[19] Gasbaoui, B., Nasri, A., Abdelkhalek, O., Ghouili, J., & Ghezouani, A. (2017). Behavior PEM fuel cell for 4WD electric vehicle under different scenario consideration. *International Journal of Hydrogen Energy*, *42*(1), 535-543.

[20] Mao, L., Jackson, L., & Jackson, T. (2017). Investigation of polymer electrolyte membrane fuel cell internal behaviour during long term operation and its use in prognostics. *Journal of Power Sources*, *362*, 39-49.

[21] Hong, P., Xu, L., Li, J., & Ouyang, M. (2017). Modeling and analysis of internal water transfer behavior of PEM fuel cell of large surface area. *International Journal of Hydrogen Energy*, *42*(29), 18540-18550.

[22] Ahmed, D. H., & Sung, H. J. (2017). Water and thermal management in PEMFCs–influencing parameters and operational conditions: A Review. *Journal of Alternative and Renewable Energy Sources*, *3*(1), 1-43.

[23] Jeon, D. H., Greenway, S., Shimpalee, S., & Van Zee, J. W. (2008). The effect of serpentine flow-field designs on PEM fuel cell performance. *International journal of hydrogen energy*, *33*(3), 1052-1066.

[24] Jithesh, P. K., Bansode, A. S., Sundararajan, T., & Das, S. K. (2012). The effect of flow distributors on the liquid water distribution and performance of a PEM fuel cell. *International journal of hydrogen energy*, *37*(22), 17158-17171.

[25] Khazaee, I. (2015). Experimental investigation and numerical comparison of the performance of a proton exchange membrane fuel cell at different

channel geometry. *Heat and mass transfer*, *51*(8), 1177-1187.

[26] Zhang, J., Tang, Y., Song, C., Xia, Z., Li, H., Wang, H., & Zhang, J. (2008). PEM fuel cell relative humidity (RH) and its effect on performance at high temperatures. *Electrochimica Acta*, *53*(16), 5315-5321.

Biography

Iman Khazaee is an associated professor of Mechanical Engineering at Shahid Beheshti University, Tehran, Iran. He received his Ph.D. in 2012 from mechanical engineering department, Ferdowsi University of Mashhad, Iran. Currently, he is working on PEM fuel cells and their optimization. He has published more than 50 articles in well-recognized journals, books, and proceedings.

Hamid Sabadbafan holds a master's degree in energy systems engineering from shahid Beheshti university in 2016. He is currently working at the Qazvin Thermal Power Plant. He has published more than 3 articles in well-recognized journals.